Ultrathin MoS_2 wrapped N-doped carbon coated cobalt nanospheres for OER application

Ashish Gaur, [a]Parrydeep K Sachdeva, [a]Rajinder Kumar,[a] Takahiro Maruyama, [b]Chandan Bera,[a] and Vivek Bagchi[a]*

a. Institute of Nano Science and Technology, Phase-10, Sector-64, Mohali, Punjab 160062, India

b. Department of Applied Chemistry, Meijo University, 1-501 Shiogamaguchi, Tempaku, Nagoya 468-8502, Japan.

*Corresponding author: vivekbagchi@gmail.com, bagchiv@inst.ac.in

Electronic Supplementary Information

S1.1 PXRD spectra of the Co-MOF

S1.2 PXRD spectra of MoS_2 and Co@NC with JCPDS stacking

S2. Raman spectra of Co@NC@MoS_2 and Co@NC

S3. BET surface area analysis of Co@NC@MoS_2

S4.1. SEM elemental mapping of Co@NC.

S4.2. EDAX analysis of the as synthesized catalyst Co@NC@MoS_2

S5.1. XPS wide scan survey spectrum of catalyst and HR spectra of Mo 3P, and N1s

S5.2. Deconvoluted peak parameters of the XPS analysis.

S5.3. Elemental percentage obtained from XPS analysis

S6. Comparative table of electrochemical properties of recently reported Co@NC based electrocatalyst.

S7.1 HRTEM analysis of catalyst after durability test

S7.2 PXRD spectra of catalyst after durability test

S8.1. LSV curve of pristine Co-BDC MOF and Co@NC@MoS_2

S8.2. ECSA normalized LSV curves of Co@NC@MoS_2 and Co@NC

S8.3. Durability test of Co@NC

S8.4. CV of all the catalysts for C_{dl} calculations.

S9. Theoretical studies

S1.1 PXRD spectra of as synthesized Co-MOF

The XRD pattern was obtained in the 2θ angular region of 5° to 30° with an increment of 0.00190/Step.

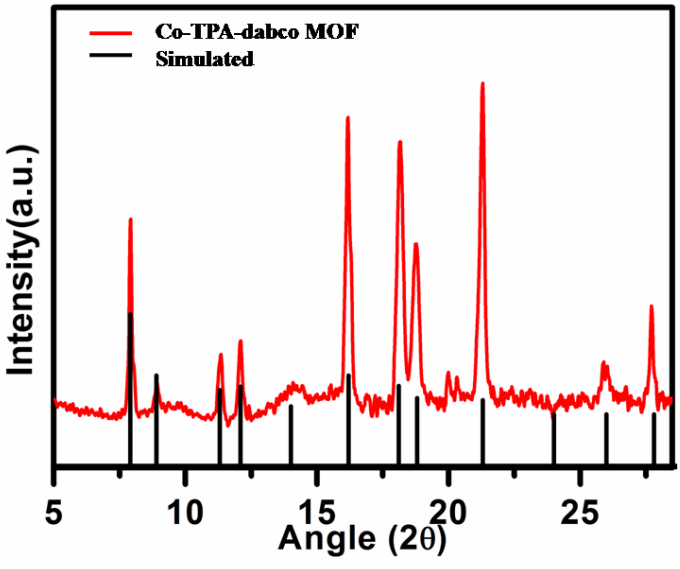

Figure S1. PXRD spectrum of Co-DABCO-BDC-MOF

S1.2. PXRD spectra of MoS_2 and Co@NC with JCPDS stacking

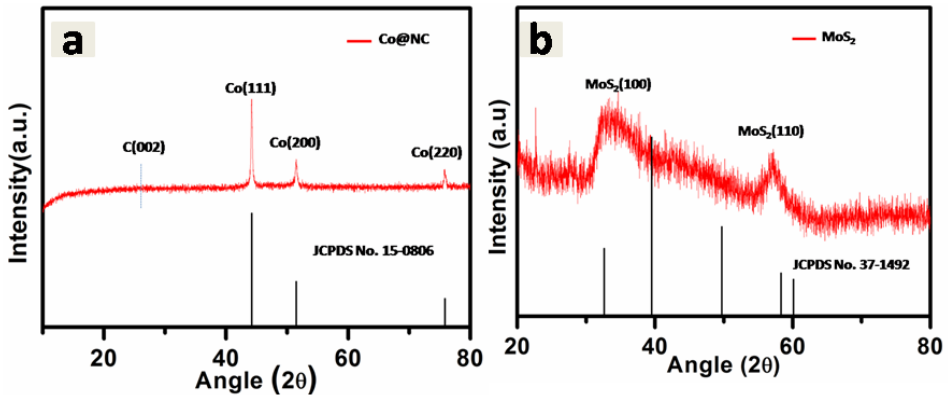

Figure S2. PXRD spectrum of MoS_2 and Co@NC with corresponding JCPDS file

S2. Raman spectrum of Co@NC and Co@NC@MoS_2.

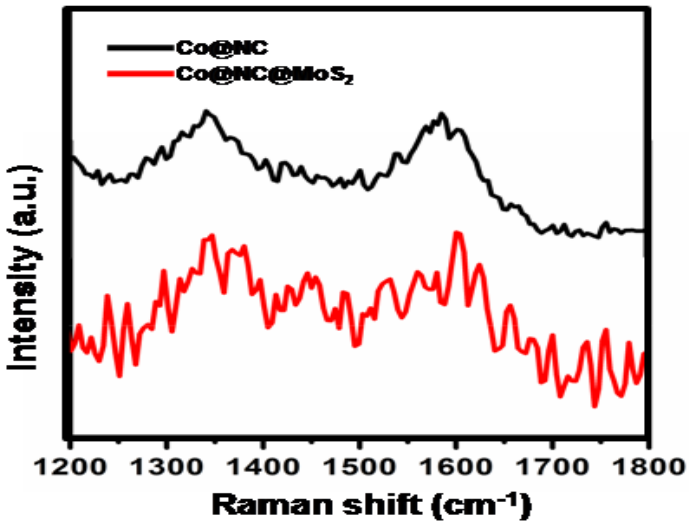

Figure S3 Raman spectroscopy showing the presence of graphitic carbon in the both Co@NC and Co@NC@MoS_2

S3. BET surface area analysis of Co@NC@MoS_2

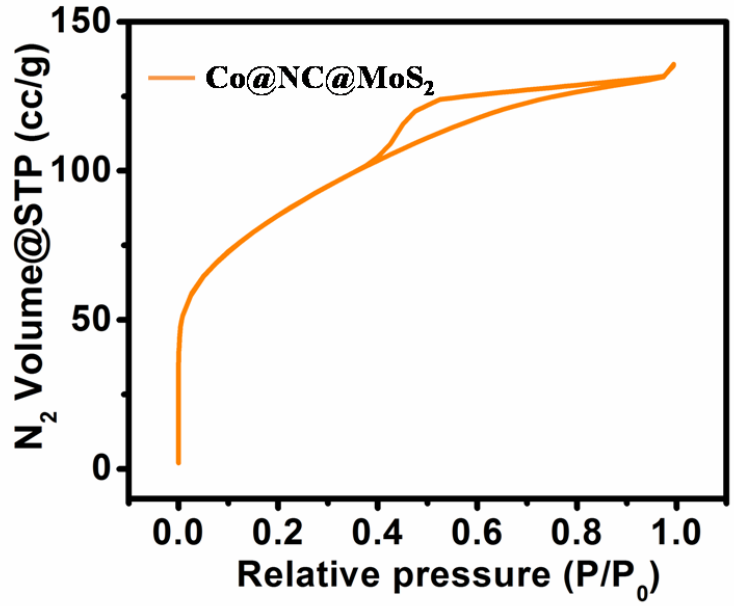

Figure S4 BET of Co@NC@MoS_2

S4.1. SEM elemental mapping of Co@NC precursor

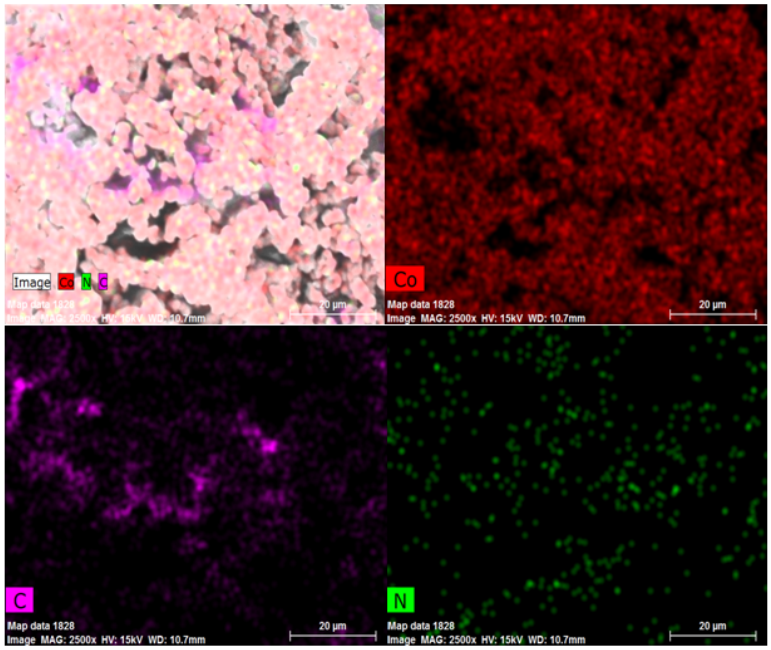

Figure S5 Elemental mapping of Co@NC show the presence of Co, C and N in the catalyst distributed uniformly throughout the sample.

S4.2. EDAX analysis of the as synthesized catalyst Co@NC@MoS_2

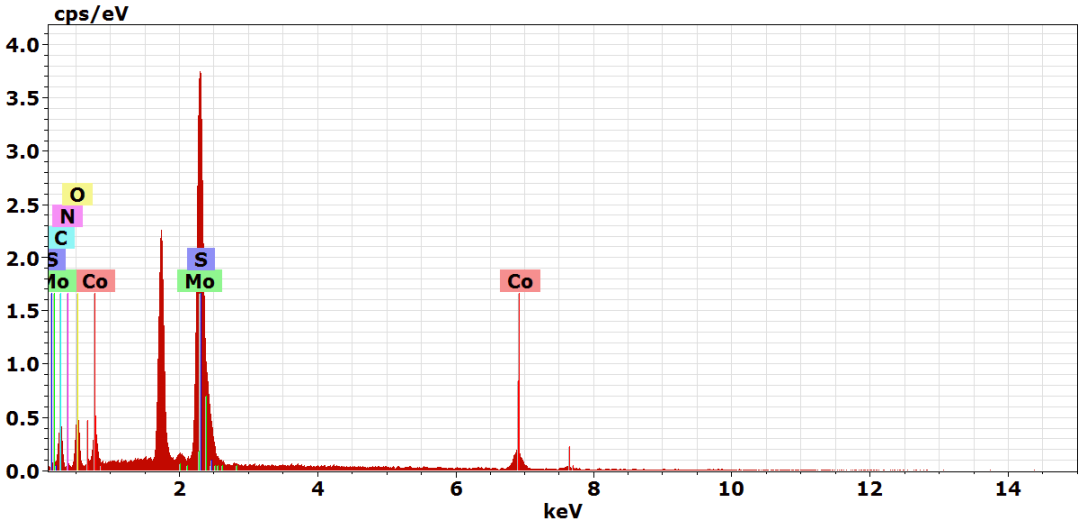

Figure S6. EDAX spectrum of Co@NC@MoS_2 the unlabeled peak in the spectrum is of Si as the analysis was carried out on silicon wafer.

S5.1. XPS wide range spectra of Co@NC@MoS_2 and HR spectra of N1s

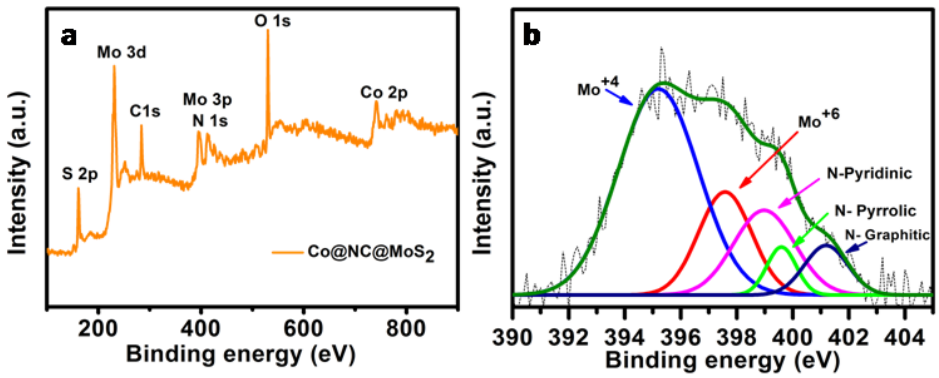

Figure S7 (a) XPS wide angle spectrum of Co@NC@MoS_2 the spectrum consist of Mo, S , O, Co, N and C elements present in the catalyst **(b)** The deconvoluted XPS spectra of N1s overlapped with Mo 3p

S5.2. Table containing the various parameters obtained after the dencovolution of XPS spectra.

Element	Peak	BE (eV)	FWHM	Area (%)
Mo 3d	Mo^{4+} Mo^{6+} S 2s	228.7and 231.8 234.6 and 235.2 225.6	1.7 and 1.8 2.0 and 2.06 1.7	23.7 and 51.9 10.5 and 10.6 3.2
S 2p	S^{2-} S^{2-}(bridging)	261.4 and 162.6 163.7	1.66 and 1.28 2.30	56.09 and 22.58 21.32
C 1s	C=C/C-C C-O/C-N C=O	284.4 286.2 288.5	2.674 2.638 2.312	59.7 24.6 15.6
Co 2p	Co(o) Co-N Co^{+2} Co^{+3}	778.8 779.6 781.5 783.3	1.78 1.77 1.78 1.76	17.24 25.50 30.43 20.07
Mo 3p& N1s	Mo^{4+} Mo^{6+} N-Pyridinic N-Pyrrolic N- Graphitic	395.1 397.5 398.9 399.5 401.1	3.37 2.24 2.57 1.24 1.8	53.74 17.82 16.84 4.59 6.98

Table S1 Deconvoluted peak parameters of the XPS analysis

S5.3. Elemental percentage obtained from XPS analysis.

Elements	Atomic %
Mo	16.21
S	33.94
C	20.24
N	7.23
Co	15.14
O	7.04

Table S2 Elemental percentage obtained from XPS analysis

S6 Comparative table of the electrochemical activity of previously reported Co@NC and MoS_2 based catalyst

Material	Electrolyte	Substrate	Overpotential (10 mA cm^{-2})	Tafel slope	Reference
Co@NC800	0.1 M KOH	GCE	371 mV	61.4 mV/dec	1
CoA@CNC700	0.1 M KOH	RDE	460 mV	-	2
Co@NPC-H	1 M KOH	RDE	350 mV	57.1 mV/dec	3
Cs-Co/C-1000	1 M KOH	GCE	290	70 mV/dec	4
MoS_2QDs	1M KOH	GCE	370	39 mV/dec	5
Co-MoS_2/BCCF-21	1M KOH	Carbon cloth	260	85 mV/dec	6
Co@NC@MoS_2	**1 M KOH**	**GCE**	**297**	**70 mV/dec**	**This work**

Table S3 Comparative table of electrochemical properties of recently reported Co and MoS_2 based electrocatalyst.

S7.1 after stability analysis of the catalyst Co@NC@MoS_2 using High resolution TEM

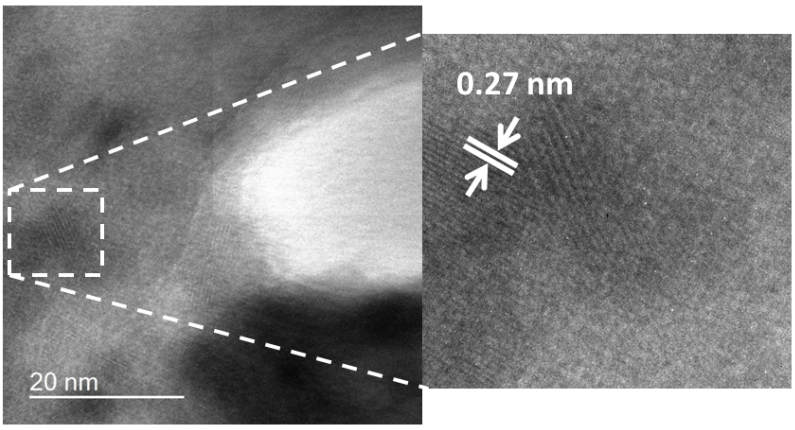

Figure S8 HRTEM images of Co@NC@MoS_2 catalyst after the durability test.

S7.2 After stability analysis of the catalyst Co@NC@MoS_2 using PXRD

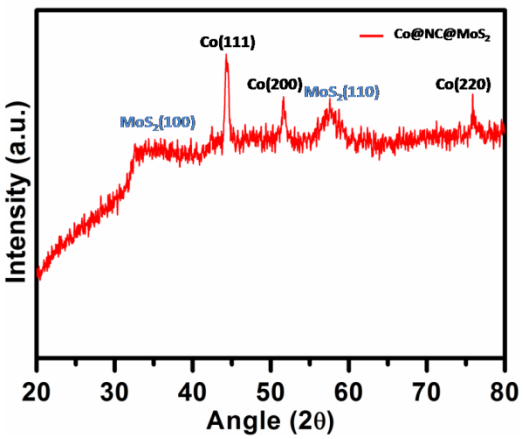

Figure S9 PXRD of the catalyst after 10 hr of stability

S8.1. LSV curve of pristine Co-TPA-BDC MOF and Co@NC@MoS_2

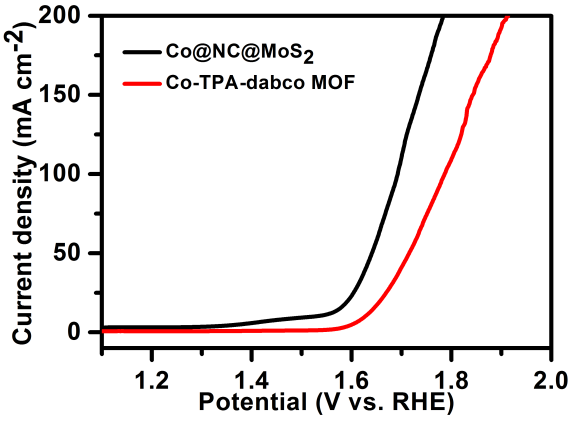

Figure S10. Comparison of the LSV of the pristine MOF and Co@NC@MoS_2

S8.2. ECSA normalized LSV curves of Co@NC@MoS_2 and Co@NC

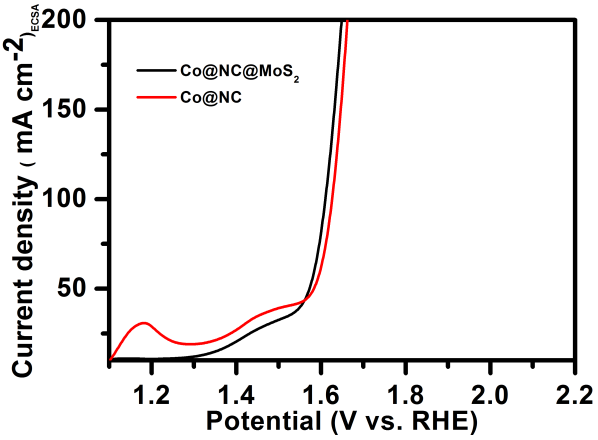

Figure S11 ECSA normalised OER activity of Co@NC@MoS_2 and Co@NC

S8.3. Stability test of Co@NC

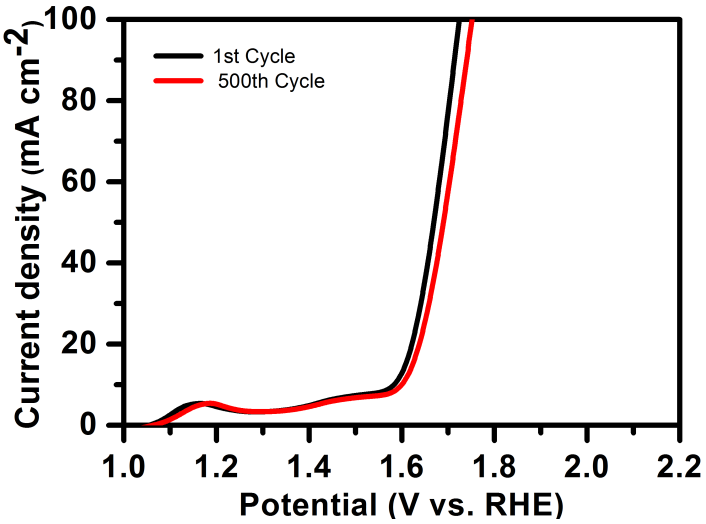

Figure S12. Durability test of Co@NC using GCE in 1M KOH

The durability test for the precursor Co@NC was done by continuously running 500 linear sweep voltammetry cycles. The significant change in the overpotential was found after 500 LSV cycles depicting the less stability of the precursor Co@NC.

S8.4. Cyclic voltammetry curve of Co@NC@MoS_2 ,Co@NC and MoS_2 in non faradic region

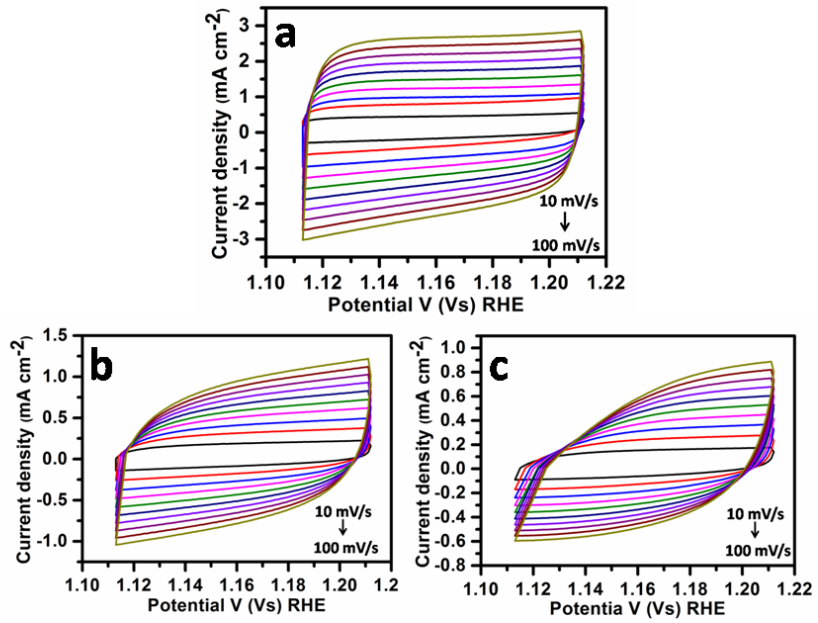

Figure S13 Cyclic voltammetry curve of (a) Co@NC@MoS_2, (b) Co@NC and (c) MoS_2 for the calculation of C_{dl}

S9 Theoretical details

Density functional theory has been used to simulate theoretical models to observe the different active sites for O* and OH* adsorption on the Co@NC@MoS_2 heterostructure. Here, we present the detailed steps to understand the OER mechanism , which is a four electron transfer process.

$$H_2O\ (l) + *\ \leftrightarrow\ OH^* + H^+ + e^- \qquad (1)$$

$$OH\ *\ \leftrightarrow\ O^*\ + H^+ + e^- \qquad (2)$$

$$O^* + H_2O\ (l)\ \leftrightarrow\ OOH^* + H^+ + e^- \qquad (3)$$

$$OOH\ *\ \leftrightarrow\ * + O_2 + H^+ + e^- \qquad (4)$$

where * stands for an active site on the surface of heterostructure. O * , OH * and OOH * are adsorbed intermediates.Gibbs energy determines whether a process will be spontaneous or not. For each step, Gibbs energy can be calculated as

$$\Delta G_1 = \Delta G(OH^*) - \Delta G(H_2O) + KT\ln a_{H^+} - eU$$

$$= E(OH^*) - E(*) - [E(H_2O) - 1/2E(H_2)] + \Delta ZPE - T\Delta S + KT\ln a_{H^+} - eU \qquad (5)$$

$$\Delta G_2 = \Delta G(O^*) - \Delta G(OH^*) + KT\ln a_{H^+} - eU$$

$$= E(O^*) - E(OH^*) + 1/2E(H_2) + \Delta ZPE - T\Delta S + KT\ln a_{H^+} - eU \qquad (6)$$

$$\Delta G_3 = \Delta G(OOH^*) - \Delta G(O^*) + KT\ln a_{H^+} - eU$$

$$= E(OOH^*) - E(O^*) - [E(H_2O) - 1/2E(H_2)] + \Delta ZPE - T\Delta S + KT\ln a_{H^+} - eU \qquad (7)$$

$$\Delta G_4 = \Delta G(*) + \Delta G(O_2) - \Delta G(OOH^*) + KT\ln a_{H^+} - eU$$

$$= E(*) - E(OOH^*) + 4.92 + [2E(H_2O) - 1/2E(H_2)] + \Delta ZPE - T\Delta S + KT\ln a_{H^+} - eU \qquad (8)$$

Here, K is Boltzmann constant, a_{H^+}represents the activity of protons, U is the potential at the electrode and e is the charge transferred. At standard conditions(pH= 0, T=298.15 K) and U =0,Gibbs energies reduce to

$\Delta G_1 = \Delta G(OH^*) - \Delta G(H_2O)$

$= E(OH^*) - E(^*) - [E(H_2O) - 1/2E(H_2)] + \Delta ZPE - T\Delta S$ (9)

$\Delta G_2 = \Delta G(O^*) - \Delta G(OH^*)$

$= E(O^*) - E(OH^*) + 1/2E(H_2) + \Delta ZPE - T\Delta S$ (10)

There exists a universal scaling relationship between OH* and OOH* ,that is

$$E_{ads}(OOH^*) = E_{ads}(OH^*) + 3.2 \text{ [1]}$$

This means the energy difference between OH* and OOH* is constant and hence,independent of the binding strength to the surface. In terms of free energy, the scaling relationship becomes

$\Delta G_3 = -\Delta G_2 + 3.2$ [1] (11)

The process of electrolysis : H_2O (l)$\rightarrow 1/2O_2$ (g) + H_2(g) requires potential of 4.92 eV. As this process involves 4 steps, the potential required for charge transfer is same for each step and equals to 1.23 eV.

Therefore,Gibbs energy for 4the step can be calculated as

$\Delta G_4 = 4.92 - (\Delta G_1 + \Delta G_2 + \Delta G_3)$ (12)

Also, $\Delta ZPE - T\Delta S$ is unknown for the adsorption on O* and OH* on the heterostructure and therefore, assumed to be zero. E(*), E(O*), E(OH*), E(H_2O), E(H_2) are the energies calculated using DFT .The calculated adsorption energies of O* and OH* on different surfaces/sites are reported in Table.S1.

Table S4. Total energy of adsorbtion of O atom and OH molecule.

S.No.	**Surface**	**Total Energy (eV)**	**E ads (eV)**	**Bond length (Å)**
1.	MoS_2+O	-68.76584279	+1.26	d(Mo1-O) = 1.99 d(Mo2-O) = 1.89 d(Mo3-O) = 1.89

2.	MoS_2+OH	-71.93280111	+0.55	d(Mo1-O) = 2.16 d(Mo2-O) = 2.16 d(Mo3-O) = 2.05 d(O-H) = 0.99
3.	Co@NC+O (N-site)	-190.49062787	+1.42	d(N-O) = 1.83
4.	Co@NC+O (C-site)	-190.69369699	+1.21	d(C1-O) = 1.90 d(C1-O) = 1.71
5.	Co@NC+OH (N-site)	-195.59675697	-1.24	d(N-O) = 1.83 d(O-H) = 0.98
6.	Co@NC+OH (C-site)	-195.38499636	-1.02	d(C1-O) = 1.90 d(C1-O) = 1.71 d(O-H) = 0.98
7.	Co@NC@MoS2 + O (O on MoS2)	-242.87172627	-2.82	d(Mo -O)= 1.75
8.	Co@NC@MoS2+OH (OH on MoS2)	-246.27386288	-3.77	d(Mo -O)= 1.91 d(O-H) = 1.01

Table S5. Enthalpies of adsorbates participating in the OER process:

Surface	**Total Energy (in eV)**
H_2O	-14.876580475
H_2	-6.88852316
H	-3.44426158
O_2	-9.27246678
H	-4.63623339
OH	-7.08922806

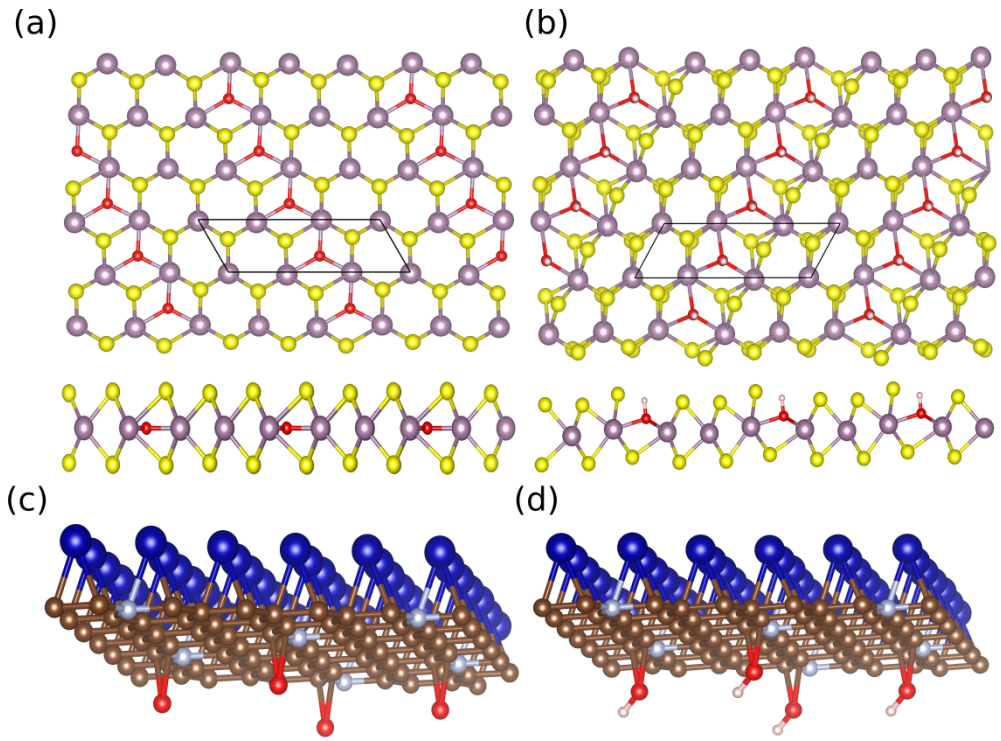

Figure S14. Atomic configurations of the intermediates adsorption O* and OH* on $MoS_2$and Co@NC surfaces. (a), (b) represent the top and side views of the adsorption on MoS_2 and (c), (d) represent the lateral views of adsorption on Co@NC surface.

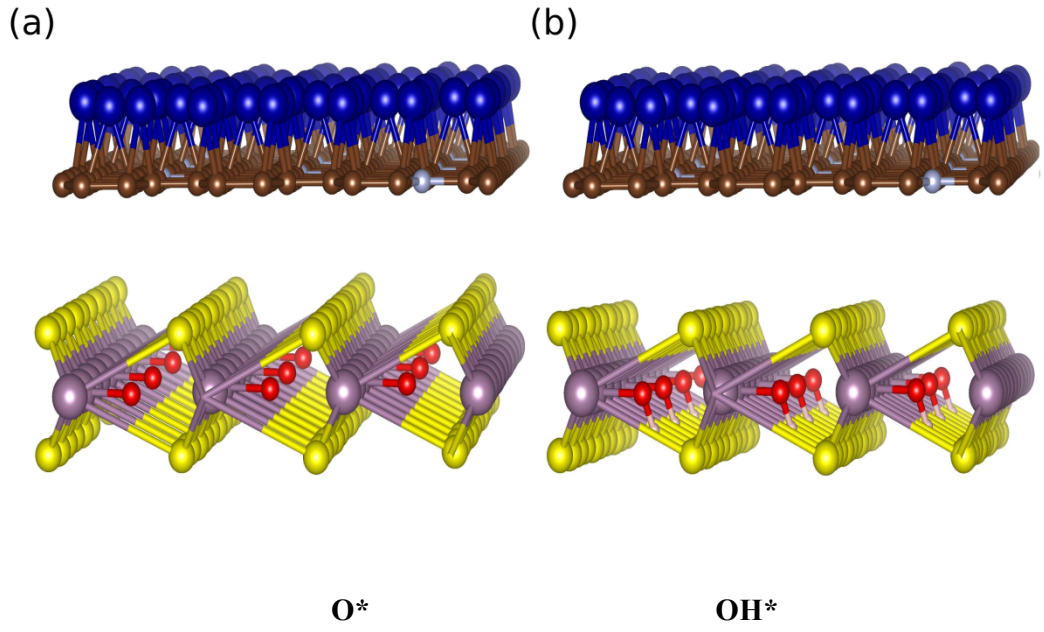

Figure S15 . Atomic configurations of the intermediates adsorption (a) O* and (b) OH* on Co@NC@MoS2 heterostructure.

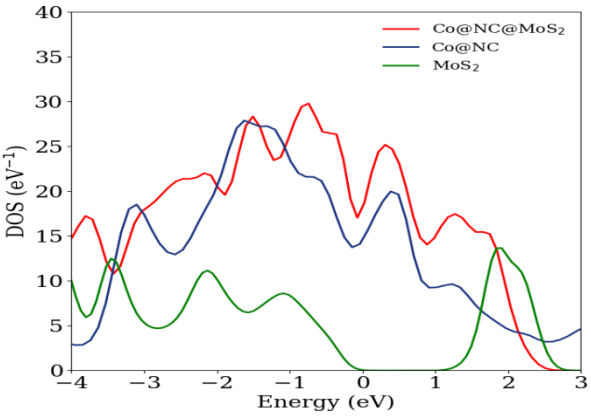

Figure S16 Calculated density of states for MoS_2,Co@NC and CO@NC@MoS_2 systems

References

[1] Su, Yunhe, et al. "Cobalt nanoparticles embedded in N-doped carbon as an efficient bifunctional electrocatalyst for oxygen reduction and evolution reactions." *Nanoscale* 6.24 (2014): 15080-15089.

[2] Shen, Mengxia, et al. "Nanocellulose-assisted synthesis of ultrafine Co nanoparticles-loaded bimodal micro-mesoporous N-rich carbon as bifunctional oxygen electrode for Zn-air batteries." *Journal of Power Sources* 450 (2020): 227640.

[3] Hou, Ya-Nan, et al. "Designed synthesis of cobalt nanoparticles embedded carbon nanocages as bifunctional electrocatalysts for oxygen evolution and reduction." *Carbon* 144 (2019): 492-499.

[4] Zhao, Jujiao, et al. "Cobalt nanoparticles encapsulated in porous carbons derived from core–shell ZIF67@ ZIF8 as efficient electrocatalysts for oxygen evolution reaction." *ACS applied materials & interfaces* 9.34 (2017): 28685-28694.

[5] Mohanty, Bishnupad, et al. "MoS2 quantum dots as efficient catalyst materials for the oxygen evolution reaction." *Acs Catalysis* 8.3 (2018): 1683-1689.

[6] Xiong, Qizhong, et al. "Cobalt covalent doping in MoS2 to induce bifunctionality of overall water splitting." *Advanced materials* 30.29 (2018): 1801450.

[7] Man, I.C., Su, H.- Y., Calle- Vallejo, F., Hansen, H.A., Martínez, J.I., Inoglu, N.G., Kitchin, J., Jaramillo, T.F., Nørskov, J.K. and Rossmeisl, J. (2011), Universality in Oxygen Evolution Electrocatalysis on Oxide Surfaces. ChemCatChem, 3: 1159-1165.